Optimal foraging of benthic diatoms evolving novel movement behaviours

Wen-Si Hu[1], Ming-Ji Huang[2], He-Peng Zhang[2], Feng Zhang[3], Wim Vyverman[4], and Quan-Xing Liu[1,5,*]

1. State Key Laboratory of Estuarine and Coastal Research, School of Ecological and Environmental Sciences, East China Normal University, Shanghai 200241, China

2. Department of Physics and Astronomy & Institute of Natural Sciences, Shanghai Jiao Tong University, Shanghai 200240, China

3. Department of Ecology, School of Resources and Environmental Engineering, Anhui University, Hefei 230601, China

4. Laboratory of Protistology and Aquatic Ecology, Department of Biology, Ghent University, Ghent 9000, Belgium

5. Shanghai Key Lab for Urban Ecological Processes and Eco-Restoration & Center for Global Change and Ecological Forecasting, School of Ecological and Environmental Sciences, East China Normal University, Shanghai 200241, China

*To whom correspondence should be addressed. Email: qxliu@sklec.ecnu.edu.cn

Adaptive locomotion of living organisms contributes to their competitive abilities and help maintain their fitness in diverse environments. To date, understanding of searching behaviours and how microscale dynamics scale up to ecosystem-level processes remain poorly understood in ecology. Here, we investigate the motion patterns of the biofilm-inhabiting marine diatom *Navicula arenaria* var. *rostellata* at the two-dimensional space. We report that individual *Navicula* cells display a novel "rotational run-and-reversal" movement behaviour at different concentrations of dissolved silicate (dSi). Using experimental measurements of the search behaviours, we show that translation motions of cells can be predicted exactly with a universal model—the generalized Langevin theoretical model. Both the experimental and theoretical results reveal quantitative agreement with an optimal foraging strategy and show that circular and reversal behaviours both contribute to comparable spatial diffusion properties. Our modelling results suggest that the evolving movement behaviours of diatom cells are driven by optimization of searching their physical surroundings, and predicted behavioural parameters coincide with the experimental observations. These optimized movement behaviours are an evolutionarily stable strategy to cope with environmental complexity.

Keywords: foraging behaviour, diatoms, ESS, rotational diffusion, reversal behaviour

One sentence summary: Contrary to wide belief, new experiments reveal that diatoms can active search food in their physical surroundings by adjusting movement behaviours.

The motion behaviours of organisms in natural world is of crucial importance to their life cycle and survival (1-4). Plants may adapt their shape and inclining position to weaken the competition between them, grow toward a more favourable light environment and collectively increase production per unit land area at high density (5), while most animals and many microorganisms can actively move from one place to another to seek favourable habitats (6), nourishment, sexual partners (7), or to escape from predators (8,9). For example, white blood cells are attracted by inflammatory signals (10), while bacteria move toward higher concentrations of sugars. At a large scale, foraging animals explore their environment to search food using their senses (2). These movements appear to be random in space and time, whereas there exist a universal principle and a unique behaviour to cope with a stressful environment. In past decades, numerous studies addressed movement behaviour of living organisms, in particular whether organism's movement patterns correspond to Brownian walks or Lévy walks (11-13). Contrary to the popular consensus that Brownian walks characterize movement of most organisms, recent studies identified its counterpart Lévy walks/flights as a universal movement pattern at different scales, ranging from molecular entities (14), swimming and swarming prokaryote and eukaryote microorganisms, foraging animals and human motion (11,15,16).

These studies have focused on unravelling the universal Lévy statistics because it accelerates the spatial diffusive potential (17,18). However, in realistic scenarios, many species of living organisms have some characteristic movement behaviour to cope with their complex surroundings (19,20). The most thorough studies of motility at the cellular scale include the swimming motions of *Escherichia coli* starting from seminal work of Howard Berg in the 1970s (21,22). It moves in almost straight runs that are interrupted by

tumbles with an average angle of about 60°, so-called ‘run-and-tumble’-like behaviour. More recently, observations of the swimming patterns of other bacteria have revealed a variety of different movement strategies (19, 23-24). Among them, the ‘run-and-reverse’ and ‘run-reverse-flick’ motion are two significant discoveries in the soil bacteria *Pseudomonas putida* (25), *Myxococcus xanthus* (26, 27), and the marine bacteria *Vibrio alginoticus* (20), respectively. Along with these experimental studies, a rich theoretical literature has addressed the different motility patterns based on concepts from the theory of random walks. These approaches are closely linked to the newly emerging research areas of active particles and microswimmers (28,29). At the same microscopical scales, many species of algal cells have active motility by self-propelled flagella to involve in translational motion and vertical migration (4,6,30). However, little is known, both from an experimental as well as a theoretical perspective, about the impact that a given movement behaviour may have on the spatial self-organization (31) and foraging of microalgae (4, 32).

Here, we report experimental observations of motility patterns of the marine benthic diatom *N. arenaria* var. *rostellata* in response to varying resource availability. Laboratory experiments revealed two key movement behaviours, including a unique two-step forward-reverse motion and rotation, respectively. We found that the diatom cells regulate the forward-backward frequencies and rotational diffusion to optimize foraging efficiency according to the ambient dSi concentration. The reversal motion is likely driven by spraying the extracellular polymeric substances (EPS) to create a new direction from forward to backward (33, 34). Our theoretical model exactly captures the diffusion scaling behaviours of mean-squared displacements (MSD) and the changes of the direction of cell

movement as observed in experimental trials. We also found that, although the reversal events and rotational diffusion appear to be random, their rates have converged to about 0.015 and 0.0054 respectively, which corresponds to the maximized efficiency of foraging. To our knowledge, these foraging traits have not been previously discussed or appreciated in microalgae, and it raises interesting relative questions about the roles of these movement behaviours on the primary productivity and biofilm formations in the benthic habitats.

Results

Movement behaviours of diatom cells. Diatom motility is involved not only in searching mating partners, but it can also direct cells towards or away from other environmental cues[6,7]. To characterise motility in *N. arenaria* var. *rostellata*, cell movement patterns were measured in a series of lab experiments in various dSi concentrations using exponentially growing cultures. Cell displacements were recorded by a Ti-E Nikon phase contrast microscope with high temporal-spatial resolutions. Trajectory analysis revealed that they display two main movement features during foraging: (i) *reversal behaviour* with a certain probability (v) under a fixed dSi concentration and (ii) continuous *rotation* on their turning angles (Fig. 1a and b, and *SI Appendix* Movie S1). The significant difference of turning behaviours suggest that diatom cells can directly response to gradient in dSi through adjusting the frequency of reversal events (see *SI Appendix* Fig. S1). This raises questions about the long-term implications to the reversal and rotational behaviours. To this end, we developed a mathematical model to show that the reversal behaviour and a minor variation in rotational noise both lead to major changes to the trajectory patterns and ultimately foraging efficiency.

Mathematical model. We utilize a discrete time model for the self-propelled diatom cells moving in a two-dimensional space. Reversal events are represented by an exponential distribution process with mean intervals derived from experimental data. Inspired by motion behaviour predictions of self-propelled rods (28), considering an Ornstein-Uhlenbeck process and standard Wiener processes on rotational diffusion, the stochastic equations of a single active cell are given by

$$x(t+\Delta t) - x(t) = V_0\, cos(\theta)\, \Delta t + \sqrt{2D_r}\, dW_1, \tag{1a}$$

$$y(t+\Delta t) - y(t) = V_0\, sin(\theta)\, \Delta t + \sqrt{2D_r}\, dW_2, \tag{1b}$$

$$\theta(t+\Delta t) - \theta(t) = \kappa(t)\omega\Delta t + \sqrt{2D_\theta} dW_3, \tag{1c}$$

$$\kappa(t+\Delta t) - \kappa(t) = -2\kappa(t)B, \tag{1d}$$

where $\kappa = \pm 1$ depicts the moving in CCW and CW orbits respectively. B is a Bernoulli random variable with success probability $\nu\Delta t$ (here ν refers the frequency of the reversal behaviours). The components of dW_1, dW_2 and dW_3 are random variables with a standard Wiener process. The cells tend to follow paths with angular speed ω. For the evolutionarily stable strategy analysis, up to 1000 cells are simulated with various prescribed rotational diffusional coefficients (noise intensity) D_θ, and fixed parameter values $V_0 = 17\ \mu m/s$, $D_r = 0\ \mu m^2/s$, $\kappa = \pm 1$, $\omega = \pi/36$ rad/s (5 degree), and $\nu = 0.02\ s^{-1}$, which are all estimated from our experiments. Note that for noncircular motion, i.e. $\omega = 0$, model (1) define a system of persistent random walks characterized by a diffusion coefficient $D = D_r + V_0^2/(2D_\theta)$ (22, 34).

To study the ensemble behaviour, we represent the configuration of diatom cells by the probability distribution functions $\Psi_\pm(\boldsymbol{r}, \theta, t)$ (28,36), here $\boldsymbol{r} = (x, y)$, which evolve

according to the Fokker-Planck equation associated with the Langevin equations (1**)**. The evolution is described by the conservation equation

$$\frac{\partial \Psi_{\pm}}{\partial t} + \nabla \cdot (\dot{\boldsymbol{r}} \Psi_{\pm}) + \frac{\partial}{\partial \theta}\left(\dot{\theta} \Psi_{\pm}\right) = \nu(\Psi_{\mp} - \Psi_{\pm}), \tag{2}$$

with $\dot{\boldsymbol{r}} = \pm V_0 \boldsymbol{e}(\theta) - D_r \nabla \log \Psi_{\pm}$, $\dot{\theta} = \pm\omega - D_\theta \frac{\partial}{\partial \theta} \log \Psi_{\pm}$. To demonstrate the validity of our theoretical model (1), we obtained the expected change in orientation and mean-square displacements (MSDs) over time from Eq. (2) and compared them directly with our experiments and numerical simulations. Thus, we can obtain the analytical expression of the time-dependent change in orientation and MSDs of the moving cells derived from Eq. (2) (see *Materials and Methods* for details).

We can obtain the time-dependent expected change in orientation of diatom cells by multiplying Eq. (2) with $\cos \Delta\theta$ and separately by $\kappa \sin \Delta\theta$ respectively, and then integrating both equations over θ and $\boldsymbol{r}$. By solving a linear system of ordinary differential equations for $\langle \kappa \cos \Delta\theta \rangle(t)$ and $\langle \kappa \sin \Delta\theta \rangle(t)$ (*SI Appendix for the derivation details*), the analytical prediction of direction change is given by

$$\langle \cos \Delta\theta \rangle(t) = e^{-(D_\theta + \nu)t}\left(\cos \sqrt{\lambda}\nu t - \frac{1}{\sqrt{\lambda}} \sin \sqrt{\lambda}\nu t\right), \tag{3}$$

where $\langle \cdot \rangle = \int_{\Omega} dA_r \int_0^{2\pi} d\theta (\Psi_+ + \Psi_-)$ and $\lambda = \left(\frac{\omega}{\nu}\right)^2 - 1$. To compare our model with experimental data, the qualitative results are shown in Fig. 2b where experimental data of orientation change decay overtime are in good agreement with our prediction Eq. (3). Theoretically, we can further obtain the analytical predictions of the time-dependent MSDs and effective diffusion coefficient from the Fokker-Planck equation (2). Using mathematical derivation, we can obtain the analytical expression as

$$\langle \Delta x^2 \rangle(t) = 4Dt + \frac{2V_0}{\nu^2(\lambda+\alpha^2)^2}\Big[(\lambda + 2\alpha - \alpha^2)\big(1 - e^{-\alpha\nu t}\cos\sqrt{\lambda}\nu t\big) + (\lambda - 2\alpha\lambda - \alpha^2)\frac{1}{\sqrt{\lambda}}e^{-\alpha\nu t}\sin\sqrt{\lambda}\nu t\Big], \quad (4)$$

where $D = D_r + \frac{V_0(\alpha-1)}{2\nu(\lambda+\alpha^2)}$, (5)

is the effective diffusion coefficient or diffusivity with $\lambda = \frac{\omega^2}{\nu^2} - 1$ and $\alpha = \frac{D_\theta}{\nu} + 1$.

Comparison between experiment and model predictions. To validate the rationality of model (1), we tested the model in the context of the movement scaling behaviours at lower cell density to ignore cell encounters modifying cell movement. In the experimental setup, low densities of individuals were used in order to minimize effects of cell-cell interactions (i.e., the attraction pheromone ref. 7). We tracked the motion of cells in two-dimensional space where cells can freely forage within given arena (*Materials and Methods*). The model predicts the individuals foraging trajectories that coincide with the experimentally observed trajectories using the experimentally determined rotational diffusion coefficient $D_\theta \approx 5.4 \times 10^{-3}$ rad^2/s (see Fig. 1 and *SI Appendix* Movie S1 and S2). Although the theoretical model (1) gives a constant speed rather than a fluctuating speed, it does not affect spatial dispersal and temporal correlation. Hence, for modelling simplicity, a constant movement behaviour is adequate to describe diatom motion.

In order to quantitatively verify our model, we conducted simulations of diatom movements with $D_\theta = 0.1$ rad^2/s, $D_\theta = 0.0054$ rad^2/s (the experiment data), and $D_\theta = 0.0001$ rad^2/s , and comparing their MSDs and the average temporal correlation $\langle \cos\Delta\theta \rangle$ with experimental results. Fig. 2a shows the two regimes of MSDs as a function of time intervals and extracted their slope k by linear fits of $\log MSD$ as function of $\log t$. For the short time scales ($t < t_C = 25\ s$), the MSDs are superdiffusive dynamics with an exponent

of $k = 2$ independent of rotational diffusion, whereas for the long times scales ($t > t_C$), the MSDs change from diffusive to subdiffusive behaviour ($k < 1$) with the simulated strength of rotational diffusion decreasing. Figures 2a clearly indicates that decreased rotational diffusion leads to a decline of slope k, indicating that the cell motion becomes circular behaviours (*SI Appendix*, Fig. S2). $k = 1.0$ corresponds to random diffusive motion without directionality, i.e. a paradigm run-and-tumble behaviour. The overall behaviours are in good agreement with experiments, numerical simulations and theoretical predictions. Note that the diffusion behaviour reverts to normal diffusions after a relative long plateau for a weak rotational diffusion coefficient (see *SI Appendix*, Fig. S3).

Fig. 2b shows the temporal correlation of cell orientation, where the positive correlation coefficient suggests the positive feedback in directional persistence, while the negative one implies a reversed motion by stochastic changes. The model accurately describes the cell reversal and rotational behaviour in both numerical simulations and theoretical predictions Eq. (3) as shown in Fig. 2, albeit the latter shows a slightly deviation from numerical simulation of angular speed ω. Specially, experimental results reveal that diatom cells display a subdiffusion to search the nutrient dSi. It is in good agreement with theoretical predictions on both MSDs and the temporal correlation of motion orientations of cells.

Optimal searching strategies in motion behaviours. Why diatoms evolve to move like this novel "circular run-and-reversal"? We hypothesize that it allows optimization of searching efficiency as a fitness proxy. We start by analysing an active cell with a sense radius r_c, blindly searching for food in an environment with a homogeneous topography. As diatoms cruise the searching space, it continuously captures nutrients that come within a capture radius r_c from the cells centre, as schematically shown in Fig. 3a. The amount of

leftover nutrients in each run shows a monotonous decline as a function of the area swept by the active cell. Here, we assume that all cells use the same strategy of reversal and rotational diffusion for the simulations. Fig. 3b plots the average amount of leftover nutrients n, obtained from 1,000 simulated trajectories as a function of various rotational diffusions, so that the decay rate τ of the exponential fitted is a rational indicator to evaluate the foraging efficiency.

We use the novel rotational diffusion and reversal as the evolvable parameter. As it can be seen in Fig. 3c, there is a remarkably peak of the foraging efficiency with evolving D_θ, but declines when rotational diffusion passes beyond a threshold. This optimal search strategy can be understood in quantitative terms by looking at the extreme cases. An individual cell in the absence of such behaviour, i.e., when $D_\theta = 0, \nu = 0$, peforms a circular walk. As D_θ decreases from the optimal peak, individuals travel probabilistically more accurately along the circle. Thus, they visit the same area frequently unless a reversal event occurs. As D_θ increases, more costs of energy are involved in the spatial dispersal processes rather than nutrients uptake, i.e., more energy is consumed to spraying EPS (see *SI Appendix*, Fig. S2). In contrast, there exists an evolvable ν-space with respect to the optimal foraging efficiency, as shown in Fig.3d. The searching efficiency decreases monotonically with increasing reversal frequency ν, but displays a wide range plateau at low reversal frequency. Thus, they optimize dispersal benefits, defined as the effective diffusivity, that asymptotically reaches a maximum value (Fig. 3d). Theoretically, our foraging efficiency τ is here comparable with the theoretical effective diffusion coefficient in Eq. (5). They predict an extreme similarity to the profile of the various rotational diffusivity and reversal events.

Qualitatively, these optimal foraging strategies as generated by the above movement traits are in accordance with observation of experimental data. Note that experimental results slightly deviate from optimal values of rotational diffusion D_θ and reversal events ν, but they only 9% and 5% underestimate comparison with the optimal values of theoretical predictions respectively. As shown in Fig. 3c and d, by comparing the numerical simulated data with analytical predictions, similar as the parameter τ, the effective diffusivity can also capture the searching efficiency of rotational and reversal behaviours. Finally, with the simulation of foraging efficiency versus various D_θ and ν, we found that there exists an optimal region where cells have maximum foraging efficiency (Fig. 4a). Interestingly, if we plot the experimental parameters overlapped with directly numerical simulations and theoretical predictions in a heatmap together, which shows the simulated foraging efficiency with respect to (D_θ, ν)-parameter space, the experimental points are in good with the optimal strategy region of Eq. **1** on the (D_θ, ν)-parameter space (cf. Fig. 4a and b).

Invasibility analysis. Individuals optimize trade-offs between the benefits of dispersal and the costs of energy involved in dSi detection because diatoms are the self-propulsive active cells. For solitary individual, individual foraging behaviours are independent of the behaviours of other individuals. Hence, the optimal foraging parameter D_θ and ν represent an evolutionary stable strategy (ESS) of the dSi detection ability (Fig. 3c and d).

We now consider populations where individual cells may encounter each other. To determine whether the optimal value is a long-term outcome of competition selection, or just be exploited by free-riding strategies (37), we created a pairwise invasibility plot (PIP, Fig. 4c) by performing an evolutionary invasibility analysis. Under a very broad range of

parameter conditions, we find that populations can convergently evolve to the ESS (Fig. 4c). The PIP reveals that diatom movement strategy of diatoms observed in our experiments is not only an evolutionarily stable strategy but also convergence stable. Here, we did not observe a branching to occur as the parameters of the model are changed in the evolutionary dynamics.

Experimental evidence of movement strategies in different dSi concentrations. To investigate the effects of different dSi concentrations on diatom foraging strategy, we performed controlled experiments to calculate the change in reversal probability and diffusion coefficient. The diatom cells move with low reversal probability and high diffusion coefficient D at intermediate dSi concentrations (from 10 to 50 mg/L), whereas low and high dSi both will lead to a decreased diffusion efficiency to cells. It is surprising that the optimal diffusion coincides with typical dSi concentrations of the most coastal water (Fig. 5a). The diffusion coefficient shows a monotonous decline with increased reversal probability (Fig. 5b). This suggests that reversal behaviour is not the single trait underlying the optimization of foraging strategy, which agrees well with our theoretical model (1) that both reversal and rotational diffusion together control the optimal searching strategy (Fig. 3 and 4).

Our results revealed that diatom cells adopt different movement behaviours with changing ambient dSi concentrations. This adaptive response suggests that diatom cells are able to sense the local dSi concentration and adjust their reversal rate to adapt to their physical surroundings. When silicon becomes the limiting factor, diatom cells increase searching activity to meet their dSi demand for survival and mitotic division. Consequently, a high diffusion coefficient induces diatom cells to explore larger areas to take up dSi.

Discussion

We have observed a novel "circular run-and-reversal" behaviour in the marine biofilm-inhabiting diatom *Navicula arenaria* var. *rostellata*. The stochastic model describing this behaviour is derived from experimental observations. Our experimental and theoretical results demonstrated that the reversal and rotational behaviours play a crucial role in optimizing searching strategies. Diatoms can maximize their foraging efficiency by changing their reversal probability and rotational noise in a silicon-limited environment. Additionally, diatoms can alter their movement strategy when resource availability changes. Rather than foraging, they suppress their effective diffusivity in a nutrient-rich condition by reduced motility, contributing to reduce the costs associated with mitotic reproduction.

The searching efficiency within a low nutrient environment is strongly dependent on cell movement behaviours. Extending our results beyond dSi scavenging, there may other attractors server as the same role to impact motion behaviours of diatoms. For instance, *in silico* comparison of the experimental data led to the speculation that diatoms have a more efficient behavioural adaptation to pheromone gradients as compared to dSi (38). Together, integrating the effect of multiple attractors into evolutionary strategies remain a fascinating topic for the future research. Our model provides a universal paradigm to understand the ecologically relevant functions of movement behaviour from the perspective of foraging theory.

Especially, insight into the movement behaviour of microorganisms in aquatic environments has been generated from disciplines such as biophysics (39-41), but the focus of these studies has largely been on the statistical physical causes of behaviour and not the

ultimate cause. Cases of reversal behaviour were reported independently in different species of marine bacteria (20, 42, 43). Recently, studies suggested that this reversal behaviours can contribute to increase efficiency bacterial foraging (20, 41) and group social effects (43), but similar evidence is still lacking for motile microalgae. This study underscores the need to study the significance of these questions in other microorganisms.

Methods

Algal cell culture and images acquisition. The *Navicula arenaria* strain 0488 is maintained in the BCCM/DCG diatom culture collection at Ghent University, http://bccm.belspo.be/about-us/bccm-dcg. It was isolated in January 2013 from high-nitrate intertidal flats of Paulina Schor, The Netherlands (51°21'N, 3°43'E). The isolate has since been maintained in unialgal culture in artificial seawater medium Aquil (f/2+Si).

The diatom cells were grown using a standard protocol. One months before the experiment, the diatom was acclimated to 2000 Lux light intensity with a light dark cycle of 12:12 hours (INFORS HT Multitron pro, Switzerland). A 100 ml flask suspension was grown on a shaker at 20°C rotating with 100 rpm. Mid–exponential–phase cells were diluted with filtered autoclaved seawater and introduced into the test chamber for observations.

In order to obtain long time data and prevent water evaporation, we put the suspension into a transparent, sterilized polymer coverslip microchannel (μ-Slide I 0.2; Ibidi, Martinsried, Germany). The channel length is 50 mm, height is 0.2 mm, and channel area is about 2.5 cm^2. The transparent channel can provide a static state hydrodynamic environment. We used Ti-E Nikon phase contrast microscope to record the pictures. We

recorded a series of continuous data under the 4-fold objective for 4 hours at a rate of 4 frames per second in the centre of the channel.

Numerical simulations. The parameters of the simulation correspond to Fig. 3c and d, Fig. 4a. For each D and ν, 1000 trajectories of 600 sec have been simulated using a time-step $\delta t = 0.1$ sec with the parameter values $V_0 = 17\,\mu m/s$, $D_r = 0\,\mu m^2/s$, $\kappa = \pm 1$, $\omega = \pi/36$ rad/s. The 'cells' move in a homogeneous space with randomly distributed nutrients ($n = 1000$). At each step, the 'nutrients' that come within a capture radius r_c from the cell centre will be removed.

Calculation of time-dependent orientation correlation and MSDs of moving cells. We computed the average temporal correlation as follows: $\langle \cos \Delta\theta \rangle(\Delta t) = [\langle v(t+\Delta t) \cdot v(t) \rangle - \langle v \rangle^2]/(\langle v^2 \rangle - \langle v \rangle^2)$, and caculated the mean square displacement via $\mathrm{MSD}(\Delta t) = \langle |r(t+\Delta t) - r(t)|^2 \rangle$.

Data avialability

The supplementary movies S1 and S2 are available from author homepage (http://www.quan-xinglab.org/publications.html). The experimental data and Matlab code used to generate Figure 1-5 are archived in a dryad public repostory (https://datadryad.org/).

Acknowledgments

This paper is a product of the project "Coping with deltas in transition" within the Programme of Strategic Scientific Alliances between China and The Netherlands (PSA) financed by the Chinese Ministry of Science and Technology (2016YFE0133700), and the National Natural Science Foundation of China (41676084).

References

1. de Jager, M., Weissing, F. J., Herman, P. M. J., Nolet, B. A. & van de Koppel, J. Lévy Walks evolve through interaction between movement and environmental complexity. *Science* **332**, 1551-1553 (2011).
2. Viswanathan, G. M. *The Physics of Foraging: An Introduction to Random Searches and Biological Encounters* (Cambridge Univ. Press, 2011).
3. Vogel, S. *Life in Moving Fluids: The Physical Biology of Flow* (Princeton Univ. Press, 1994).
4. Houghton, I. A., Koseff, J. R., Monismith, S. G., & Dabiri, J. O. Vertically migrating swimmers generate aggregation-scale eddies in a stratified column. *Nature* **556**, 497-550 (2018).
5. López, P. M., Sadras, V. O., Batista, W., Casal, J. J., & Hall, A. J. Light-mediated self-organization of sunflower stands increases oil yield in the field. *Proc. Natl Acad. Sci. USA* **114**, 7975-7980 (2017).
6. Bondoc, K. G. V., Heuschele, J., Gillard, J., Vyverman, W., & Pohnert, G. Selective silicate-directed motility in diatoms. *Nat. Commun.* **7**, 10540 (2016).
7. Bondoc, K. G. V. *et al.* Decision-making of the benthic diatom *Seminavis robusta* searching for inorganic nutrients and pheromones. *ISME J.* **9**: inpress (2018). doi: 10.1038/s41396-018-0299-2
8. Biewener, A. A. *Animal Locomotion* (Oxford University Press, 2003).
9. Ros, I. G., Bassman, L. C., Badger, M. A., Pierson, A. N., & Biewener, A. A. Pigeons steer like helicopters and generate down- and upstroke lift during low speed turns. *Proc. Natl Acad. Sci. USA* **108**, 19990 (2011).
10. Harris, T. H. *et al.* Generalized Lévy walks and the role of chemokines in migration of effector CD^{8+} T cells. *Nature* **486**, 545-548 (2012).
11. Zaburdaev, V., Denisov, S., & Klafter, J. Lévy walks. *Rev. Mod. Phys.* **87,** 483-530 (2015).
12. Raposo, E. P., Buldyrev, S. V., da Luz, M. G. E., Viswanathan, G. M., & Stanley, H. E. Lévy flights and random searches. *J. Phys. A-Math Theor.* **42,** 434003 (2009).
13. Chubynsky, M. V., & Slater, G. W. Diffusing diffusivity: A model for anomalous, yet Brownian, diffusion. *Phys. Rev. Lett.* **113,** 098302 (2014).

14. Chen, K., Wang, B., & Granick, S. Memoryless self-reinforcing directionality in endosomal active transport within living cells. *Nat. Materials* **14,** 589-593 (2015).
15. Ariel, G., *et al.* Swarming bacteria migrate by Lévy walk. *Nat. Commun.* **6,** 8396 (2015).
16. Humphries, N. E., Weimerskirch, H., Queiroz, N., Southall, E. J., & Sims, D. W. Foraging success of biological Lévy flights recorded in situ. *Proc. Natl Acad. Sci. USA* **109,** 7169-7174 (2012).
17. del-Castillo-Negrete, D. Truncation effects in superdiffusive front propagation with Lévy flights. *Phys. Rev. E* **79,** 031120 (2009).
18. de Jager, M., *et al.* How superdiffusion gets arrested: Ecological encounters explain shift from Lévy to Brownian movement. *Proc. Roy. Soc. B* **281,** 20132605 (2014).
19. Stocker, R. Reverse and flick: Hybrid locomotion in bacteria. *Proc. Natl Acad. Sci. USA* **108,** 2635-2636 (2011).
20. Xie, L., Altindal, T., Chattopadhyay, S., & Wu, X.-L. Bacterial flagellum as a propeller and as a rudder for efficient chemotaxis. *Proc. Natl Acad. Sci. USA* **108,** 2246-2251 (2011).
21. Berg, H. C. & Brown, D. A. Chemotaxis in *Escherichia coli* analysed by three-dimensional tracking. *Nature* **239,** 500 (1972).
22. Berg, H. C. *Random Walks in Biology* (Princeton Univ. Press, 1993).
23. Johansen, J. E., Pinhassi, J., Blackburn, N., Zweifel, U. L., & Hagström, Å. Variability in motility characteristics among marine bacteria. *Aquatic Microbial Ecology* **28,** 229-237 (2002).
24. Gutierrey-Medina, B., Guerra, A. J., Maldonado, A. I. P., Rubio, Y. C., & Meza, J. V. G. Circular random motion in diatom gliding under isotropic conditions. *Phys. Biol.* **11,** 066006 (2014).
25. Theves, M., Taktikos, J., Zaburdaev, V., Stark, H., & Beta, C. A bacterial swimmer with two alternating speeds of propagation. *Biophys. J.* **105,** 1915-1924 (2013).
26. Wu, Y. L., Kaiser, A. D., Jiang, Y., & Alber, M. S. Periodic reversal of direction allows *Myxobacteria* to swarm. *Proc. Natl Acad. Sci. USA* **106,** 1222-1227 (2009).
27. Avraham, B., Strain, S. K. , Hernández, R. A., Eshel, B.-J., & Florin, E.-L. Periodic reversals in *Paenibacillus dendritiformis* swarming. *Journal of Microbiology* **195,** 2709-2717 (2013).

28. Takagi, D., Braunschweig, A. B., Zhang, J., & Shelley, M. J. Dispersion of self-propelled rods undergoing fluctuation-driven flips. *Phys. Rev. Lett.* **110,** 32-44 (2013).
29. Sokolov, A., Apodaca, M. M., Grzybowski, B. A. , & Aranson, I. S. Swimming bacteria power microscopic gears. *Proc. Natl Acad. Sci. USA* **107,** 969-974 (2010).
30. Sengupta, A., Carrara, F., & Stocker, R. Phytoplankton can actively diversify their migration strategy in response to turbulent cues. *Nature* **543,** 555-558 (2017).
31. Mitchell, J. G., Pearson, L., & Dillon, S. Clustering of marine bacteria in seawater enrichments. *Appl. Environ. Microb.* **62,** 3716-3721 (1996).
32. Woodson, C. B. & McManus, M. A. Foraging behavior can influence dispersal of marine organisms. *Limnology and Oceanography* **52,** 2701-2709 (2007).
33. Lee, R. E. *Phycology* (Cambridge Univ. Press, 2008).
34. Medlin, L. K., Crawford, R. M., & Andersen, R. A. Histochemical and ultrastructural evidence for the function of the labiate process in the movement of centric diatoms. *British Phycological Journal* **21,** 297-301 (1986).
35. Großmann, R., Peruani, F., & Bär, M. Diffusion properties of active particles with directional reversal. *New J. Phys.* **18,** 043009 (2016).
36. Doi, M. & Edwards, S. F. *The Theory of Polymer Dynamics* (Oxford Univ. Press, 1988).
37. Hauert, & Christoph Cooperation, Collectives Formation and Specialization. *Advances in Complex Systems* **9,** 315-335 (2006).
38. Bondoc, K. G. V., Lembke, C., Vyverman, W., & Pohnert, G. Searching for a mate: pheromone-directed movement of the benthic diatom seminavis robusta. *Microbial Ecology* **72,** 287-294 (2016).
39. Shapiro, O. H., Kramarsky-Winter, E., Gavish, A. R., Stocker, R., & Vardi, A. A coral-on-a-chip microfluidic platform enabling live-imaging microscopy of reef-building corals. *Nat. Commun.* **7,** 10860 (2016).
40. Son, K., Menolascina, F., & Stocker, R. Speed-dependent chemotactic precision in marine bacteria. *Proc. Natl Acad. Sci. USA* **113,** 8624-8629 (2016).
41. Son, K., Guasto, J. S., & Stocker, R. Bacteria can exploit a flagellar buckling instability to change direction. *Nature Phys.* **9,** 494-498 (2013).
42. Magariyama, Y., *et al.* Difference in bacterial motion between forward and backward swimming caused by the wall effect. *Nat. Commun.* **88,** 3648-3658 (2005).

43. Shashi, T., Mingzhai, S., Filiz, B., Kannappan, P., & Shaevitz, J. W. Directional reversals enable *Myxococcus xanthus* cells to produce collective one-dimensional streams during fruiting-body formation. *J. Roy. Soc. Interface* **12,** 20150049 (2015).

Lists of figure captions:

Fig. 1: Experimental observations and theoretical model predictions of the main features of reversal behaviours of diatom *Navicula arenaria* var. *rostellata*. (**a**) A typical cell trajectory containing circling run and reversal behaviours captured with a microscopy at 4 frames per second (see *SI Appendix* Movie S1) for 5 min. (**b**) Cropping of the partial trajectory of the panel (a) depicts a reversal behaviour, where the running from CCW switches to CW through the reversal behaviours, and vice versa. The arrows indicate the moving direction of the cell. (**c**) Experimental data showing the movement velocity before and after a reversal occurrence; for clarity, not all speeds are shown here. (**d**) and (**e**) The spatial trajectory and the reversal event predictions are given by model (1) with parameters value V_0 =17 $\mu m/s$, $D_\theta = 0.0054$ rad^2/s, $\nu = 0.02$, and $\omega = \pi/36$ rad/s. Colorbars in panel (a, d) depict the time (see *SI Appendix* Movie S2 for details).

Fig. 2: Laboratory measured and theoretical predicted diffusion behaviours of diatom cells. (**a**) Mean squared displacement (MSD) for three different values of the rotational diffusion coefficient D_θ obtained by performing a numerical simulation of model (1) and comparison with the experiments (circles symbols), respectively. By decreasing the strength of rotational diffusion in the model, the dependence of the MSD on time becomes consistent with confined diffusivity from ballistic behaviours similarly to cage-effect emergence after the characteristic times ($\sim 25\ s$). Parameters are $\omega = \pi/36$ rad/s, $\nu = 0.02$, and V_0 =17 μm/s. The dashed lines are a guide to the eye to mark the change of the scaling law, and solid line predicted by Eq. (4). (**b**) Correlation of measured and predicted changes in the direction of cells moving. Experimental data (□ symbols) have error bars

representing lower and upper SD. Corresponding predictions (solid lines and dashed lines) are given by Eq. (**3**) and numerical simulations obtained from model (1).

Fig. 3: Predicting optimal foraging strategy in spatial randomized nutrient targets and theoretical results. (**a**) Schematic representation (not to scale) of diatom cells blindly searching for randomly distributed nutrient resources (dots). The cells placed in two-dimensional space move with constant speed $\boldsymbol{V_0}$ and variable orientation described model (1). The capture radius $\boldsymbol{r_c}$ is about 20 $\boldsymbol{\mu}$m size (dashed circle area). (**b**) The distinct exponential function, $\boldsymbol{n(t) = Ae^{-\tau t}}$, with the decay rate τ describes the foraging efficiency of diatom movement strategy with respect to various $\boldsymbol{D_\theta}$ and $\boldsymbol{\nu}$. (**c, d**) The efficiency of captured nutrients as a function of $\boldsymbol{D_\theta}$ and $\boldsymbol{\nu}$, respectively. The efficiency values are averaged over 1000 trajectories at stable capture rates with various $\boldsymbol{\omega}$, where the plot is scaled to the maximum value at $\boldsymbol{D_\theta = 0.3}$ and $\boldsymbol{\nu = 0.0001}$ respectively. The solid lines represent an analytical prediction of effective diffusivity from theory Eq. **4**, coinciding with directly numerical simulations of model (1). The gray shaded area represents mean $\pm$SD around the experimentally measured values of $\boldsymbol{D_\theta}$ and $\boldsymbol{\nu}$ on species *Navicula arenaria* var. *rostellata*, respectively.

Fig. 4: Theoretical and experimental results implicate the emergence of the foraging efficiency for various behavioural strategies. (**a**) Heatmap of foraging efficiency with respect to (D_θ, ν)-parameter space obtained from spatial randomly distributed nutrient targets and constant movement speed for $\omega = \pi/36$ rad/s and $V_0 = 17$ μm/s. The optimal foraging occurs over a window of behavioural parameters of ν and D_θ, for instance, the yellow areas are the optimal foraging regions. The boundaries of the optimal regions

change sharply with increasing reversal rate (white dashed lines with intervals $\Delta\tau = 0.1$). In the low reversal rate limit, there are nonlinear effects of the rotational diffusion on diatom foraging. The colored-solid dots correspond to the experimentally measured rotational diffusion coefficients versus reversal rate on diatom *Navicula arenaria* var. *rostellata* and the colorscale indicates the scaled foraging efficiency, τ from 0 to 1.0. (**b**) Theoretical prediction of Eq. (**5)** on the effective diffusivity as functions of the rotational diffusivity and reversal events. It shows a similar spatial profile comparison with directly numerical simulations. (**c**) Pairwise invasibility plot (PIP) indicating that the movement behavioural strategy of rotational diffusivity evolves toward a stable point 0.2 (vertical dashed line). For a range of resident (*x*-axis) and mutant (*y*-axis) movement strategies, the PIP indicates whether a mutant has a higher (red) or a lower (green) fitness than the resident. Plus and minus symbols indicate strategy combinations resulting in positive and negative invasion fitness, respectively. Here, the PIP shows that the rotational diffusivity with 0.2 is the sole evolutionarily stable strategy (ESS). Parameters: $\nu = 0.02$, and $\omega = \pi/36$ rad/s.

Fig. 5: Reversal behaviour and diffusivity depend on the ambient dSi concentration. (**a**) The diffusivity of diatom cells maximizes at an ambient dSi concentration of about 30 mg/L and declines at low and high dSi concentrations. The probability of reversal events shows a sharply increase when dSi goes beyond 60 mg/L, but it maintains a plateau at low dSi. (**b**) Diffusion coefficient, showing a nonmonotonic relationship with increased reversal events, which have a maximized dispersal coefficient about $\nu = 0.02$ coincident

with theoretical predictions. The grayscale rectangle indicates the dSi concentrations in most coastal ecosystems.

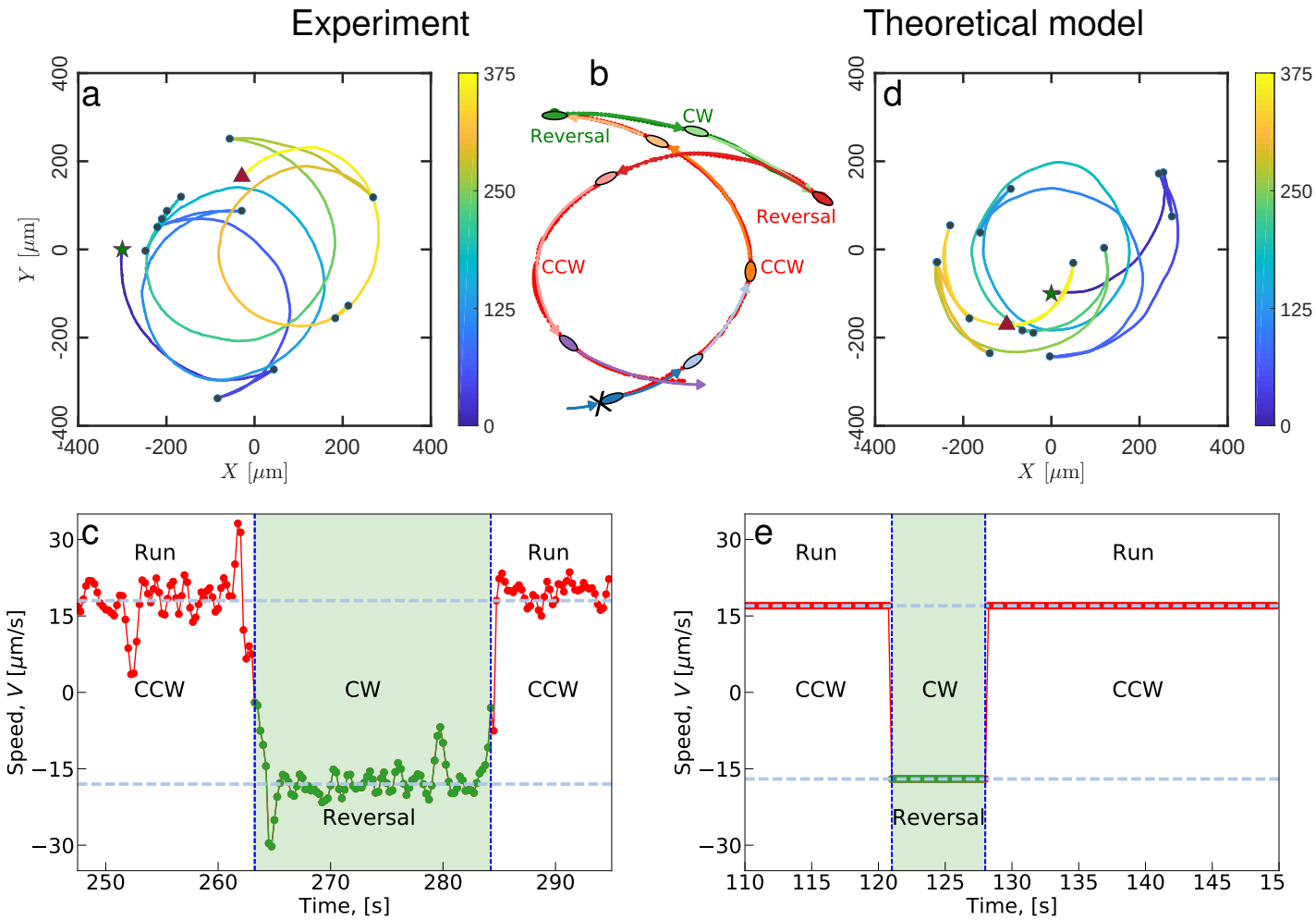

Experiment
Theoretical model
a
b
d
c
e
Reversal
CW
CCW
Run
Speed, V [μm/s]
Time, [s]
X [μm]
Y [μm]

Figure 1.

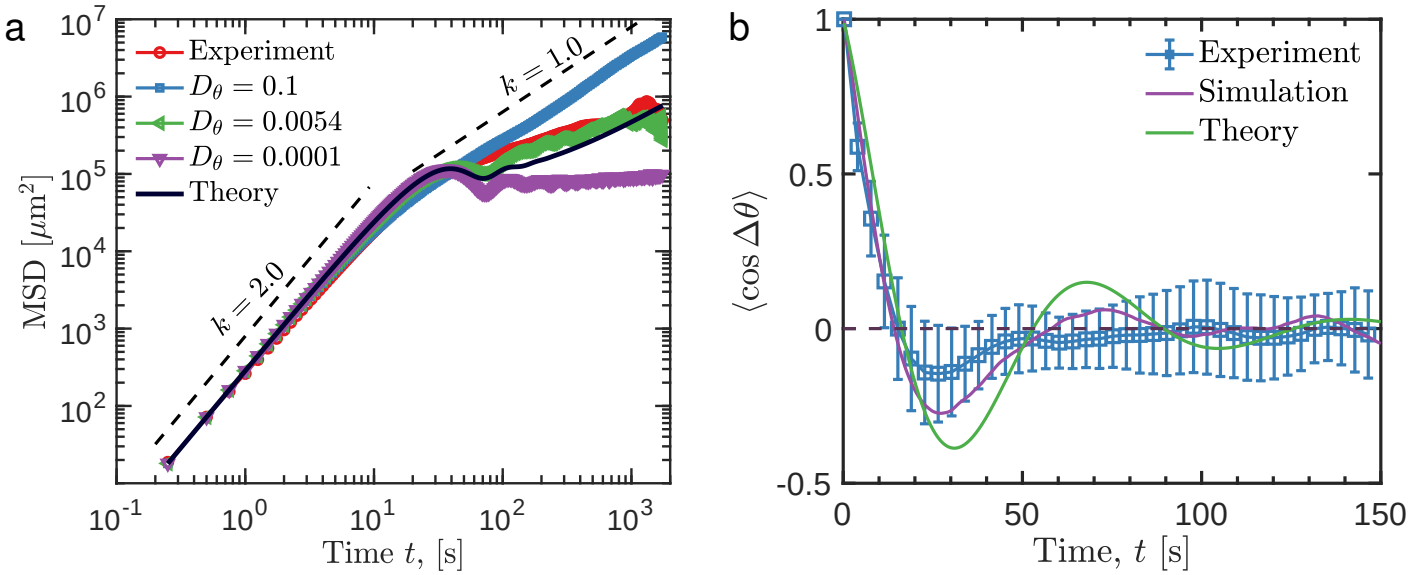
a
Experiment
$D_\theta = 0.1$
$D_\theta = 0.0054$
$D_\theta = 0.0001$
Theory
$k = 1.0$
$k = 2.0$
MSD [μm^2]
Time t, [s]
b
Experiment
Simulation
Theory
$\langle \cos \Delta\theta \rangle$
Time, t [s]

Figure 2.

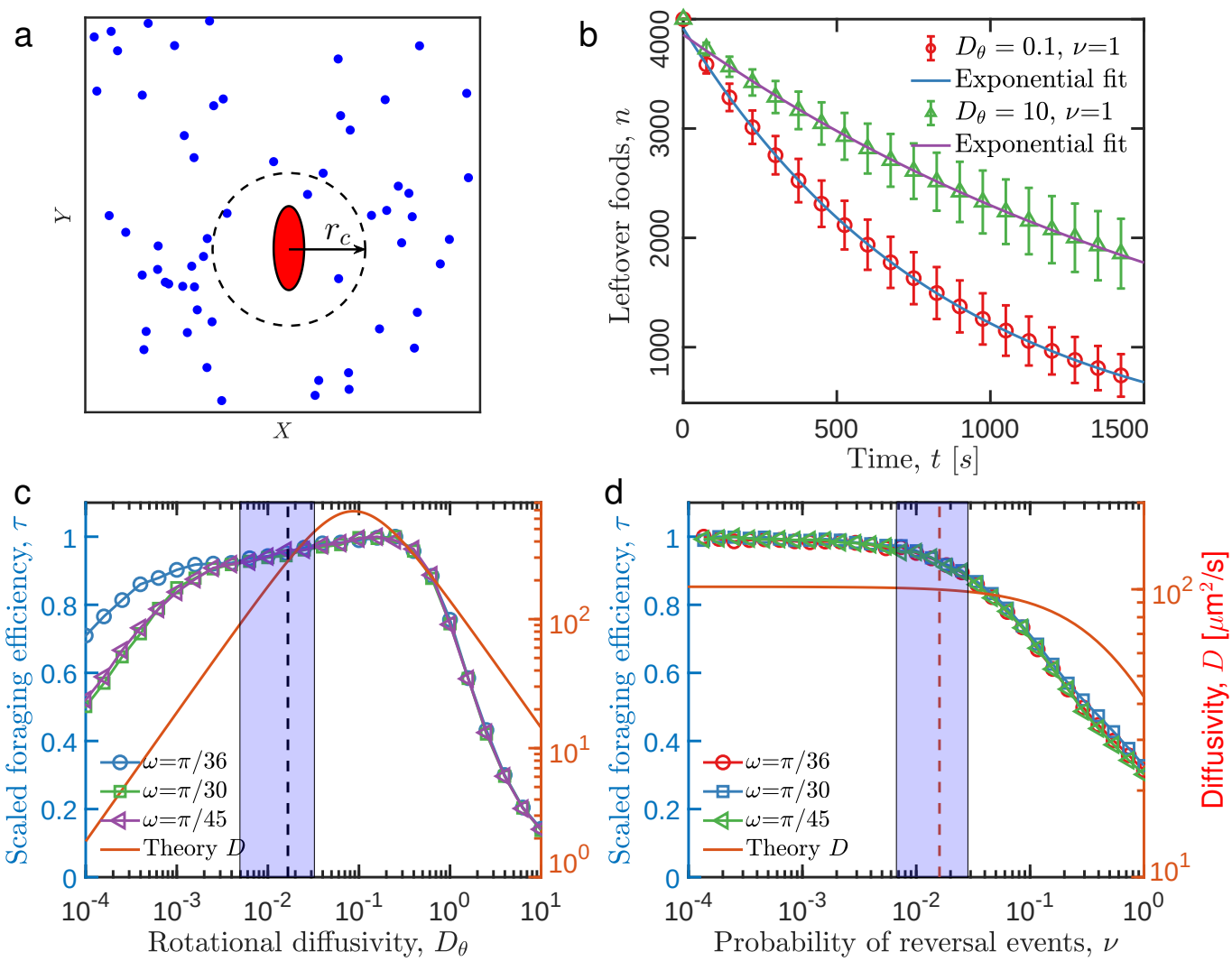
a
Y
X
r_c
b
Leftover foods, n
Time, t [s]
$D_\theta = 0.1$, ν=1
Exponential fit
$D_\theta = 10$, ν=1
Exponential fit
c
Scaled foraging efficiency, τ
Rotational diffusivity, D_θ
ω=π/36
ω=π/30
ω=π/45
Theory D
d
Scaled foraging efficiency, τ
Diffusivity, D [μm^2/s]
Probability of reversal events, ν
ω=π/36
ω=π/30
ω=π/45
Theory D

Figure 3.

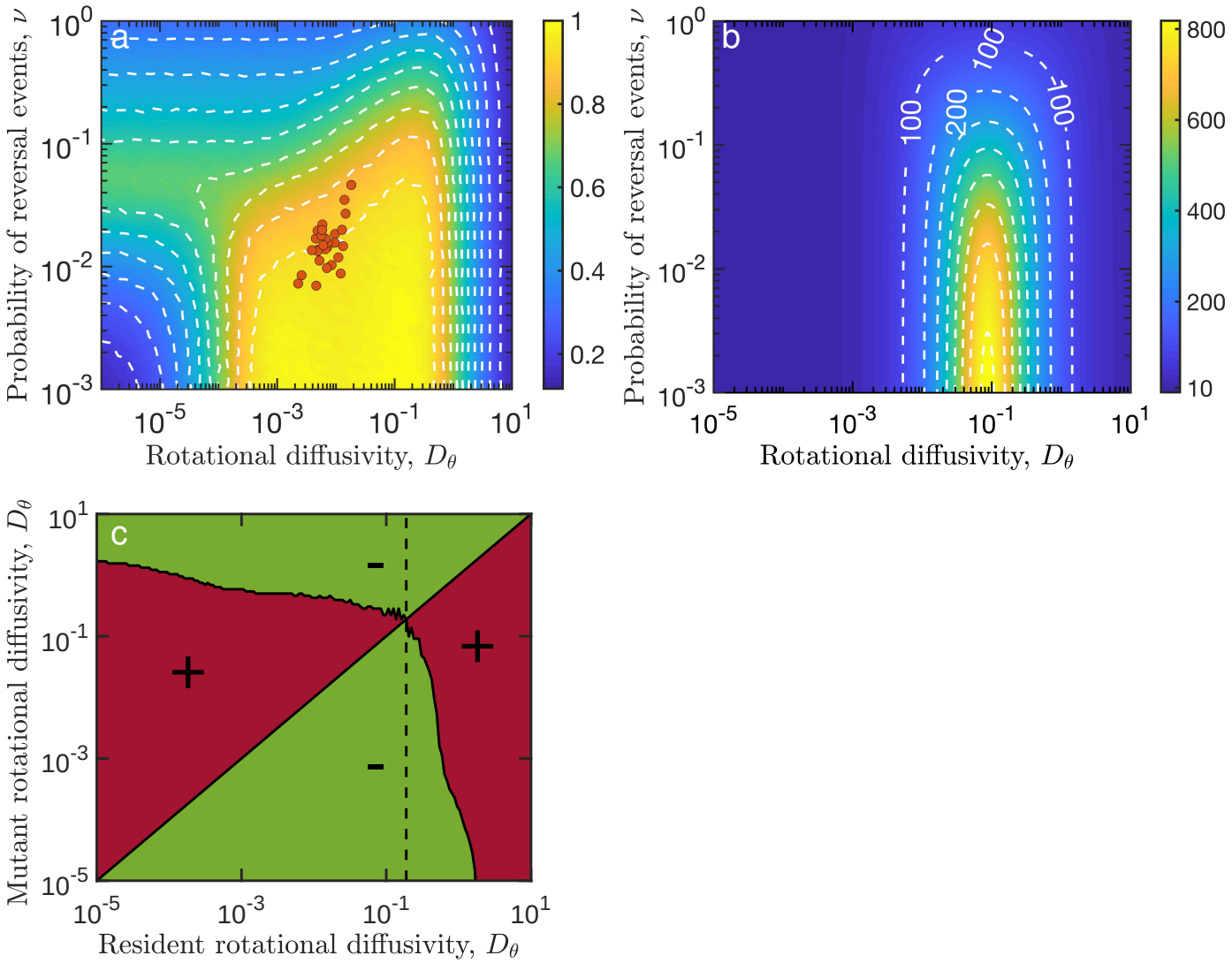
a
b
c
Probability of reversal events, ν
Rotational diffusivity, D_θ
Mutant rotational diffusivity, D_θ
Resident rotational diffusivity, D_θ
10^{0}
10^{-1}
10^{-2}
10^{-3}
10^{-5}
10^{-3}
10^{-1}
10^{1}
1
0.8
0.6
0.4
0.2
800
600
400
200
10
100
200
+
-

Figure 4.

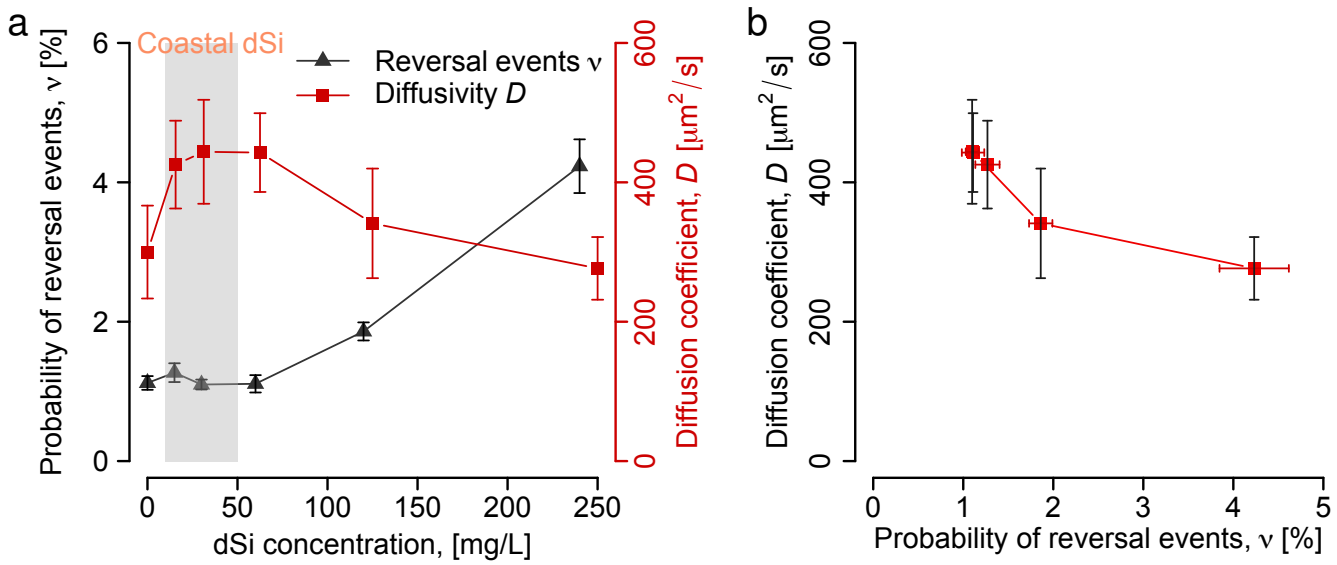
a
Coastal dSi
Reversal events ν
Diffusivity D
Probability of reversal events, ν [%]
Diffusion coefficient, D [μm²/s]
dSi concentration, [mg/L]
0
2
4
6
0
200
400
600
0
50
100
150
200
250
b
Diffusion coefficient, D [μm²/s]
Probability of reversal events, ν [%]
0
200
400
600
0
1
2
3
4
5

Figure 5.